Hull girder ultimate strength of bulk carrier (HGUS-BC) evaluation: Structural performances subjected to true inclination conditions of stiffened panel members

Imaduddin Faqih [a], Ristiyanto Adiputra [b,**], Aditya Rio Prabowo [a,*], Nurul Muhayat [a], Sören Ehlers [c,d], Moritz Braun [d]

[a] Department of Mechanical Engineering, Universitas Sebelas Maret, Surakarta, 57126, Indonesia
[b] Research Center for Hydrodynamics Technology, National Research and Innovation Agency (BRIN), Surabaya, 60112, Indonesia
[c] Institute for Ship Structural Design and Analysis, Hamburg University of Technology, Hamburg, 21073, Germany
[d] Institute of Maritime Energy Systems, German Aerospace Center, Hamburg, 21502, Germany

ARTICLE INFO

ABSTRACT

To enhance the safety of ship structure design, this study evaluated time-dependent hull girder ultimate strength considering thick corrosion and the inclination conditions of stiffened panels. The hull girder ultimate strength was calculated using incremental–iterative methods based on IACS-CSR in a bulk carrier hull model. The corrosion effect was measured as the thickness reduction in structural members, and inclination conditions were considered such as non-uniform uniaxial thrust, which influences the yield strength of structural members. The corrosion effect was investigated from 5 to 20 years of service time, wherein the corrosion rate was obtained based on a reference and was then divided into standard and severe corrosion rate conditions. The effect of non-uniform uniaxial thrust was considered the yield stress reduction on all the stiffener elements in an inclined position. The safety level of the design within each timeframe of the measured corrosion effect was then considered based on the ultimate limit state. This study found that the corrosion rate greatly affects HGUS, with severe corrosion having a greater affect than standard corrosion. In 20 years of service time with uniform loads in hogging conditions, the highest HGUS reduction caused by standard corrosion is 5.87%, while severe corrosion causes a reduction of 24.48%. Moreover, non-uniform uniaxial thrust was found to have a negative effect on HGUS, lowering the HGUS value on benchmark hull models both in hogging and sagging conditions.

Nomenclature

Symbols/ Name	Units	Description
A_{E-n50}	cm^2	Net area of stiffeners with attached plating of width b_E
A_{pE-n50}	cm^2	Net sectional area of attached plating of width b_E
A_{p-n50}	cm^2	Net sectional area of attached plating
A_{s-n50}	cm^2	Net sectional area of stiffener, without attached plating
b	m	Width of cross-section
b_c		A constant based on the ship block coefficient
b_E	m	Effective width of the attached plating
b_f	mm	Flange height

(continued on next column)

(continued)

B	m	Ship breadth
C_1, C_2		Coefficient to be determined by the statistical analysis of corrosion measurement data
C_b		Coefficient block
C_w		Wave coefficient
C_{wp}		Warping constant
d	m	Web thickness
E	N/mm^2	Modulus of elasticity
E_m	N/mm^2	Material's Young modulus
f_m		Distribution factor for vertical wave bending moment along the ship's length
f_{nl-vh}		Coefficient considering nonlinear effects applied to hogging

(continued on next page)

---

* Corresponding author.
** Corresponding author.
    E-mail addresses: ristiyanto.adiputra@brin.go.id (R. Adiputra), aditya@ft.uns.ac.id (A.R. Prabowo).

(continued)

f_{nl-vs}		Coefficient considering nonlinear effects applied to sagging
f_p		Fatigue and strength assessment coefficient
f_{sw}		Distribution factor along the ship length
F	N	Allowable load
G	N/m^2	Shear modulus
h	m	Web height
h_w	mm	Net web thickness
h_{we}	mm	Effective height of the web
I	m^4	Moment of Inertia
I_{E-n50}	cm^4	Net moment of inertia of stiffeners with attached plating of width b_{E1}
I_p	m^4	Polar moment of inertia about the shear center
I_T	m^4	St. Venant torsional constant
I_{tor}	m^4	Second moment for torsion at no restrained warping
I_w	m^6	Bimoment of cross-section
l_e	m	Effective length with respect to warping
L	m	Length of ship/column
m_{tor}		Total torsion moment
M_s	tonnes metres	Still water bending moment
M_{sw}	N/mm^2	Still-water bending moment
$M_{sw-h-min}$		Minimum Still Water Bending Moment for hogging
$M_{sw-s-min}$	N/mm^2	Minimum Still Water Bending Moment for sagging
M_u	N/mm^2	Ultimate bending moment
M_w	tonnes metres	Wave bending moment
M_{wv}	N/mm^2	Wave-induced bending moment
$M_{wv-h-mid}$	N/mm^2	Vertical wave bending moment for strength assessment in hogging
$M_{wv-s-mid}$	N/mm^2	Vertical wave bending moment for strength assessment in sagging
n		Factor counting for end conditions
r	$\sqrt{\dfrac{I}{st_p + h_w\,t_w + b_f\,t_f}}$	Radius of gyration
r_i		Non-dimensional displacement ratio (i = top or bot)
r_r	mm/year	Corrosion rate
R_{eHB}	N/mm^2	Equivalent minimum yield stress of the considered element
R_{eHp}	N/mm^2	Minimum yield stress of the material of the considered plate
R_{eHs}	N/mm^2	Minimum yield stress of the material of the considered stiffener
s	m	Spacing of the adjacent longitudinal stiffener
s_t	m	Transverse stiffeners
t	m	Flange thickness
t_f	mm	Flange thickness
t_{f-n50}	mm	Thickness of flange
t_{n50}	mm	Thickness of plate
t_p	m	Thickness of the plating
t_r	mm	Depth of corrosion (loss of plate thickness due to corrosion)
t_w	mm	Web thickness
t_{w-n50}	mm	Thickness of web
T	years	Vessel service time
T_c	years	Coating duration
T_e	years $T_e = T - T_c - T_t$	Time of exposure to the structure after coating damage
T_t	years	Duration of corrosion transition
$u_{top,bot}$		The ratio between the axial displacements exerted at the topmost and bottommost reflectively
v	m	Total displacement in y-direction
W	tonnes	Total ship weight
W_A	tonnes	Moment of the weight aft of amidships
W_F	tonnes	Moment of the weight forward of amidships
β		Slenderness ratio for plates
β_E	$10^3 \dfrac{s}{t_{n50}} \sqrt{\dfrac{\varepsilon\,R_{eHp}}{E}}$	Correction factor for effective width
β_w	$\dfrac{h_w}{t_{w-n50}} \sqrt{\dfrac{\varepsilon\,R_{eHs}}{E}}$	Correction factor for effective height

(continued on next column)

(continued)

$\gamma_u, \gamma_{sw}, \gamma_w$		Partial safety factors for M_u, M_{sw}, and M_{wv}, respectively
ε		Relative strain
θ	°	Angle of rotation was taken to vary from 0.0 to 90.0°,
$\diagup$	m	Longer side of the plate
λ		Slenderness ratio for stiffened panels
σ_0	N/mm^2	
$\sigma_{C1,2,...4}$	N/mm^2	Critical stress in for each respective buckling mode
σ_{CP}	N/mm^2	Buckling stress of attached plate
σ_{CR1}	N/mm^2	Beam column buckling of stiffeners composing the hull girder transverse section
σ_{CR2}	N/mm^2	Flexural-torsional buckling of stiffeners composing the hull girder transverse section
σ_{CR3}	N/mm^2	Web local buckling of flanged stiffeners composing the hull girder transverse section
σ_{CR4}	N/mm^2	Web local buckling of flat bar stiffeners composing the hull girder transverse section
σ_{CR5}	N/mm^2	Buckling of transversely stiffened panels composing the hull girder transverse section
σ_u	N/mm^2	Ultimate compressive strength
σ_y	N/mm^2	Material's yield stress
ϕ		Edge function

1. Introduction

Sea transportation is among the modes of transportation in highest demand due to its effectiveness, especially for mass transportation and logistics [1–6]. However, due to harsh environments and extreme loading conditions, ships and other related marine structures are vulnerable to accidents. Such conditions demand detailed safety assessments of ships and other related marine structures [7–13]. According to a report by Lloyd's List Intelligence [14], from the beginning of 2012 to mid-2021, there were 21,746 shipwrecks, 947 of which were total losses. In addition, of the total number of shipwrecks, 5% of them were caused by hull damage. In another report by the European Marine Safety Agency [15], during 2014–2020, there were 15,481 accidents on EU-flagged vessels and of all these accidents, 58 were caused by hull failure. Considering these reports, it is observed that hull failure is one of the most severe causes of accidents because it can cause hull collapse and almost certainly cause a ship to experience total loss.

Ship structures need to be safe as well as economically justifiable. Furthermore, the possible loss of human life/cargo and environmental pollution as a result of ship sinkage should lead to even higher precautions. The prevention of hull collapse is one of the most critical factors in designing and assessing the safety of ship structures. Hull collapse can occur when the maximum load-carrying capacity of the hull (hull girder ultimate strength) is not enough to withstand the load received by the hull [16]. Hull girder ultimate strength (HGUS) is the maximum bending capacity that the hull girder can withstand when subjected to longitudinal pressure. A ship's structure can be considered safe when the HGUS exceeds the total bending moment received [17].

One of the most powerful methods for predicting ultimate strength behavior with efficiency is empirical formulation. Empirical formulations can also produce precise results for ultimate compressive strength [18]. HGUS calculations are the most common empirical formulations for predicting a ship-shaped structure's ultimate strength. The calculation of HGUS was first performed by Caldwell [19], who calculated HGUS using his own formula; however, the formula proposed by Caldwell did not consider reductions in the strength of each element. Smith [20] later proposed a simplified beam-column method taking into account the elastoplastic behavior of panels and local buckling. When used in a design, such beam-column methods provide acceptable results where stiffener characteristics are dominant on the plate. Furthermore, Ueda and Rashed [21] proposed the idealized structure unit method (ISUM) to lower the degree of freedom and nodes in the system structure so as to reduce the computational time of ultimate strength analysis

under biaxial loads/thrust and lateral thrust. Currently, the HGUS determination method most widely used is Smith's method as detailed by the International Association of Classification Societies Common Structural Rules (IACS-CSR). The IACS-CSR simplifies the incremental–iterative method for evaluating HGUS using analytically derived stress–strain curves on stiffened plate, hard corners, and plate elements.

In ensuring the strength of a ship's structure, the estimation of the structural behavior of the ship throughout service time is also an important factor to consider. Considerations with respect to this factor include the roughness of the hull structure, the possibility of damage as an operating effect in the marine environment, and the possibility of degradation due to corrosion. Corrosion is defined as the destruction of a metal's surface as a result of environmental interaction [22]. Corrosion-related problems are one of the two most important factors alongside fatigue, which has the potential to cause the degradation of ship structures as ships age [23]. Corrosion can occur on unprotected surfaces of ships as well as those whose protection has been lost. Over time, corrosion can continue to grow and peel off, thus allowing the metal under it to be exposed to corrosive attacks.

Corrosion reduces the thickness of steel stiffeners and plates thoroughly on a ship's hull girders. There are many ways to overcome the effects of corrosion on metals. Inhibitors represent one of the most used techniques for preventing corrosions. There are many inhibitor types, such as 8-hydroxyquinoline, 2-[(5-methylpyrazol-3-yl)methyl] benzimidazole, (E)-4-Methoxy-N-(Methoxybenzylidene)Aniline, and (E)-N-(4-Methoxybenzylidene)-4-Nitroaniline [24–26]. Environmentally friendly inhibitors for reducing the effects of pollution have been developed, such as through the use of eucalyptus oil and basil oil [27, 28]. For application to metals, wherein the operating conditions can be severely challenging, the absorption rate of inhibitors can be increased by using halide salts such as potassium iodide or by using ion nitriding techniques [29,30]. Despite all these options, the possibility of the corrosion of metal throughout its lifetime, especially in extreme environmental conditions, remains quite likely.

Corrosion was recognized as the most common threat to the integrity of ship hull girders [31]. Almost all parts of a ship have the possibility of being exposed to the effects of corrosion. Hull girder structure comprises an assembly of such elements, and the hull cross-section decreases as a result of corrosion growth. This makes a ship more vulnerable to the vertical bending moment caused by seawater waves. Hull damage caused by excessive corrosion degradation can reach about 90% [31]. In the calculation of local stiffener buckling and its contribution to a ship's longitudinal strength, uniform thrust is often thought of as a loading condition, acting alone or together with the main shear stress and/or hydrostatic pressure. However, depending on the relative angle and vertical location of some elements with respect to the neutral axis (NA) of the center of the vessel, axial strain and axial displacement deviate from uniformity (non-uniform) [32]. Moreover, deviation can occur in the presence of the even degradation of all elements of a ship's structure due to corrosion without exceptional elements that receive non-uniform axial thrust. Such degradation allows a ship's structure to be more sensitive to non-uniform uniaxial thrusts.

As such, Anyfantis [33] tested the effect of non-uniform axial thrust on the ultimate strength of stiffened panels. It was concluded that when a stiffened panel was located close to the NA and given a non-uniform thrust, there was a 10% reduction in strength compared with calculations when using a uniform thrust. Furthermore, Anyfantis [32] carried out development on the tee stiffener using a non-uniform uniaxial thrust. Anyfantis concluded that the closer an element is to NA, the greater the influence of the relative orientation angle on HGUS.

In the process of calculating the strength of a ship's structure, it is also necessary to determine the level of safety. The calculation of the level of security in the structure of a ship is carried out by determining the ultimate limit state (ULS) of the structure. ULS design represents the failure of the structure when subjected to the maximum load value [34].

The quality of ship structure decreased as a result of corrosion and non-uniform uniaxial thrust during service time. Furthermore, this decreased quality decreased the ability of the ship structure to preserve its original conditions and prevent accidents. As a result, the safety level of the structure also decreased. Currently, few researchers have examined the combination of the effects of corrosion and non-uniform uniaxial thrust on HGUS by considering the safety level. The main objective of this study is to take into account the effect of reducing the thickness of hull girder elements as the effect of corrosion on the HGUS of hull models in two corrosion conditions, namely standard and severe. HGUS calculations are carried out using Smith's method in two load conditions, uniform axial load and non-uniform uniaxial load, as well as in hogging and sagging conditions. The HGUS value then determines the safety level of a ship's structural design using the ULS parameter. Based on the obtained HGUS results, the ULS value is calculated and compared to existing rules. By understanding the extent to which the effects of corrosion and non-uniform uniaxial thrust affect the structure of a vessel, accidents pertaining to ship and maritime structure could be minimalized.

2. Milestone study

Several researchers have conducted research on several factors that later became the basis of this paper. Some of these researchers are referenced in Table 1. Anyfantis [32,33] conducted researches on uniaxial thrust and stiffened panels and concluded that uniaxial thrust had a negative effect on the yield strength of stiffened panels. Kim et al. [18] researched the effect of axial compression on stiffened panels. These researchers did not consider the overall ultimate strength of the ship hull. Wei et al. [35] and Shi et al. [36] focused on determining the effect of initial imperfections on the ultimate strength of ship structures. Zayed et al. [31] and Paik et al. [37] created a time-dependent corrosion model for the hull plates of ship structure. Adiputra et al. [17] used the reliability approach to investigate the effects of structural and load uncertainties on hull girder ultimate strength.

3. Hull reference model

The hull reference model used in this study was a bulk carrier. The cross-section of the model obtained from the International Ship and Offshore Structures Congress 2000 (ISSC-2000) [38] is shown in Fig. 1. The bulk carrier model cross-section in Fig. 1 has 324 stiffened panels, with 90 of them subject to non-uniform thrust due to their inclination condition.

4. Hull girder ultimate strength

In this research, to obtain data on the influence of corrosion severity and the use of non-uniform uniaxial thrust, HGUS calculation methods were used. HGUS calculation methods were chosen on the basis that one of the most powerful methods for predicting ultimate strength behavior with efficient effort is empirical formulation. Empirical formulations can also produce precise results for ultimate compressive strength [18].

There are many kinds of HGUS calculation methods. One method that is quite widely used and has been simplified in the International Association of Classification Societies Bulk Carrier (IACS-BC) is Smith's method. In calculating HGUS using Smith's method, the hull cross-section is divided into individual element structures where each element has an influence on the value of HGUS. The structure of these elements is categorized into stiffener elements, stiffened plate elements, and hard corner elements [39].

- Beam column buckling

$$\sigma_{CR1} = \phi \sigma_{C1} \frac{A_{s-n50} + A_{pE-n50}}{A_{s-n50} + A_{p-n50}} \tag{1}$$

Table 1

Summarized references of milestone studies.

Authors [Year]	Title	Objective	Results
Konstantinos N. Anyfantis [33]	Ultimate compressive strength of eccentrically loaded stiffened panels in ship structures: a computational study	To conduct a preliminary study on the effect of uneven axial thrust on the ultimate strength of a given stiffener	When the stiffener plate is near the neutral axis of the midship section and a suitable non-uniform thrust is applied, a 10% reduction in strength is observed compared with respective predictions made considering uniform thrust.
Konstantinos N. Anyfantis [32]	Ultimate strength of stiffened panels subjected to non-uniform thrust	The evaluation of the ultimate strength of stiffening panels in hull structures subjected to compound uniaxial shear in-plane and out-of-plane bending moments. This problem is generalized by introducing a non-uniform thrust described by displacement ratio and rotation angle and by introducing an aspect ratio.	The stiffened panels' orientation affects their ultimate strength when studied under non-uniform compression conditions the closer they are to the ship section's neutral axis. A formula for refining a ship's ultimate bending capacity is proposed along with a basis for performing refined local buckling checks on stiffened panels.
Ristiyanto Adiputra, Takao Yoshikawa, and Erwandi [17]	Reliability-based assessment of ship hull girder ultimate strength	A reliability approach is used to investigate the effects of structural and load uncertainties on the estimation of ship hull girder reliability. Randomness in material properties, geometric properties, initial geometric imperfections, and corrosion behavior are all examples of structural uncertainties. Uncertainties about the load include statistical uncertainties, model uncertainties, environmental uncertainties, and nonlinearity uncertainties.	According to the reliability indexes, the sagging condition is more vulnerable than the hogging condition, and the ship could be safely operated for 25 years under the standard corrosion rate scenario but only 15 years under the severe corrosion rate scenario.
A. Zayed, Y. Garbatov, and C. Guedes Soares [31]	Corrosion degradation of ship hull steel plates accounting for local environmental conditions	To introduce a simplified method for estimating corrosion degradation in various ship spaces based on	The longitudinal bulkheads between cargo tanks below 3 m from the tank's top have the lowest corrosion level. It is also

Table 1 (*continued*)

Authors [Year]	Title	Objective	Results
		limited information about these spaces' environmental conditions. Various ship spaces are classified based on the main characteristics that affect corrosion degradation. Each space is assumed to have nearly uniform properties throughout. Based on the available data, a unique corrosion model is created for each space	demonstrated that the side shell plates at the quay contact region have the most severe corrosion.
Gao Da-wei, Shi Gui-jie, and Wang De-yu [35]	Residual ultimate strength of hull structures with crack and corrosion damage	To analyze residual ultimate strength following crack damage. Simple equations using the regression method are proposed to predict the residual ultimate strength of cracked container ships. The corrosion additions ruled by three classification societies, the American Bureau of Shipping (ABS), the China Classification Society (CCS), and DET NORSKE VERITAS (DNV), are assumed to be the most severe corrosion conditions and are subtracted from build-in scantlings to obtain net scantlings. The residual ultimate strength of a container ship after corrosion damage is then determined.	The uniform corrosion has the greatest effect on hogging ultimate strength, followed by bottom modulus, sagging ultimate strength, and deck modulus. The section modulus can be used to evaluate the effect of crack damage on ultimate strength in a conservative manner. The deck modulus can be used to predict the crack effect on ultimate strength when the crack is located above the neutral axis. When the crack is located below the neutral axis, however, the bottom modulus can be used.
Gui-jie Shi, De-yu Wang, Bing Hu, and Shi-Jian Cai [36]	Effect of initial geometric imperfections on dynamic ultimate strength of stiffened plate under axial compression for ship structures	The study object is stiffened plates used in ship structures. The dynamic action is assumed to be a load with an impact velocity along the axial direction at the plate's short edge. The relationship between initial geometric	Imperfection in the initial geometry has a significant impact on dynamic ultimate strength. Incorrect initial imperfection assumed on the stiffened plate causes a 22%38% overestimation of dynamic ultimate strength. The plate slenderness ratio

(continued on next page)

Table 1 (*continued*)

Authors [Year]	Title	Objective	Results
		imperfection and higher buckling modes is investigated. The effect of initial geometry imperfection on dynamic ultimate strength is investigated using stiffened plates from ship structures under uniform compression velocity along the axial direction with the relevant stiffeners and girders represented by boundary conditions.	and strain rate are critical parameters that have a significant influence on the dynamic ultimate strength of a stiffened plate. The dynamic ultimate strength of a plate with a higher plate slenderness ratio can be lower than the yielding strength. A general procedure for considering initial geometric imperfection in dynamic ultimate strength analysis is presented. A simple formula for determining the dynamic ultimate strength of a stiffened plate is proposed.
Jeom Kee Paik, Anil K. Thayamballi, Young Il Park, and Joon Sung Hwang [37]	A time-dependent corrosion wastage model for seawater ballast tank structures of ships	To create the time-dependent reliability or risk of aging ship structures for low-alloy carbon steel plates used in the structure of ship seawater ballast tanks. Measurement data of structural wastage due to corrosion for such ship steel plates are collected, and statistical analysis is used to quantify the statistical characteristics of corrosion loss and rate in terms of ship age. The analysis of corrosion (thickness loss) measurements in terms of ship age is used to investigate the statistical characteristics (mean, variance, and distribution) of corrosion progress in steel plates used for the seawater ballast tanker structures of ships.	For the most likely (average) corrosion characteristics, the relative frequency distribution of the annualized corrosion rate may follow the Weibull function, whereas for upper bound (severe) corrosion characteristics, this rate is closer to the normal function. The annualized corrosion rate of seawater ballast tanks is in the range of 0.0466–0.0823 mm/year for the most likely (average) corrosion trends using all the corrosion measurements collected, but the upper bound (severe) corrosion values representing the 95% and above band of the corrosion data can be three or more times higher.
Do Kyun Kim, Hui Ling Lim, and Su Young Yu [18]	A technical review on ultimate strength prediction of stiffened panels in axial compression	The ultimate strength of a stiffened panel is calculated using an empirical formulation supported by a thorough review	As the ultimate compressive strength increased, so did the ultimate tensile strength. In other words, empirical formulations and

Table 1 (*continued*)

| Authors [Year]	Title	Objective	Results
		of the subject. The formulation's accuracy is compared with numerical simulation results. A total of 10,500 stiffened panel cases are evaluated, with changes in plate and stiffener geometry taken into account and modelled and analyzed with ANSYS nonlinear finite element method (NLFEM) to obtain an ultimate strength dataset subjected to longitudinal compression. Only the average level of plate initial deflection and stiffener element initial distortion are considered.	design formulations can predict the decreasing tendency but not the fluctuation behavior. In the case of a software-based analytical method, ALPS/ULSAP may better predict ultimate strength behavior based on the findings of the statistical analysis.
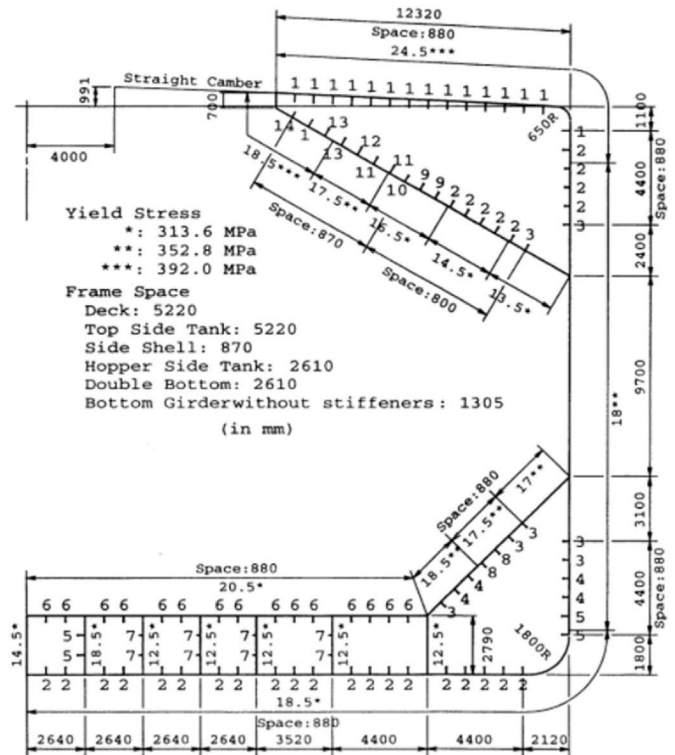
Fig. 1. Hull girder cross-section of the International Ship and Offshore Structures Congress (ISSC)-2000 bulk carrier [38].

where σ_{C1} is critical stress due to compression. The σ_{C1} based on IACS-BC is equal to:

$$\sigma_{C1} = \frac{\sigma_{E1}}{\varepsilon} \text{ for } \sigma_{E1} \leq \frac{R_{eHB}}{2}\varepsilon \tag{2}$$

$$\sigma_{C1} = R_{eHB} \left(1 - \frac{R_{eHB}\,\varepsilon}{4\,\sigma_{E1}} \right) \text{ for } \sigma_{E1} > \frac{R_{eHB}}{2}\varepsilon \tag{3}$$

where σ_{E1} follows Euler column buckling stress and is described as:

$$\sigma_{E1} = \pi^2 E \frac{I_{E-n50}}{A_{E-n50}l^2} 10^{-4} \tag{4}$$

Eq. (4) was based on the Euler column formula. In column buckling, the Euler column formula predicts the critical buckling load of a long column with pinned ends. The Euler column formula was stated as:

$$F = \pi^2 n \frac{E\,I}{L^2} \tag{5}$$

where n was the factor accounting for the end conditions: $n = 1$ for a column pivoted at both ends; $n = 4$ for both ends fixed; $n = 2$ for one end fixed and the other end rounded; and $n = 0.25$ for one end fixed and one end free. Considering column buckling occurs in long columns with pinned ends, the n value used was 1. Based on this, buckling columns could be formulated into the following:

$$\sigma = \pi^2 \frac{E\,I}{L^2} \tag{6}$$

- Torsional buckling

$$\sigma_{CR2} = \phi \frac{A_{s-n50}\,\sigma_{C2} + A_{p-n50}\,\sigma_{CP}}{A_{s-n50} + A_{p-n50}} \tag{7}$$

As σ_{C1} was the buckling beam column, σ_{C2} was the critical stress due to compression. Based on IACS-BC, σ_{C2} is equal to σ_{C1}. The main difference between torsional buckling and beam column buckling is in the value of σ_{E2}. While σ_{E1} is based on the Euler column formula, σ_{E2} is a representation of Euler torsional buckling stress. σ_{E2} in IACS-BC is formulated as follows:

$$\sigma_{E2} = \frac{E}{I_p} \left[\left(\frac{m_{tor}\pi}{l_{tor}} \right)^2 I_w.10^2 + \frac{1}{2(1+v)} I_T + \left(\frac{I_{tor}}{m_{tor}\pi} \right)^2 \varepsilon.10^{-4} \right] \tag{8}$$

Eq. (8) was based on the formulation of elastic torsional buckling stress formulated as follows:

$$\sigma_{ET} = \frac{G\,I_T}{I_p} + \frac{\pi^2\,E\,C_w}{I_p l_e^2} $$

The parameters I_T and C_w were calculated by adjusting the shape of the cross-section. The tee stiffener value I_T and C_w were formulated as stated in Det Norske Veritas [40]:

$$I_T = \frac{1}{3} \left(2\,b\,t^3 + h\,d^3 \right) \tag{9}$$

and

$$C_{wp} = \frac{h^2 b^3 t}{24} \tag{10}$$

- Web local buckling of stiffeners made of flanged profiles

Local buckling can relieve stress and liberate strain energy so that the kink or crease rapidly propagates around and along the column, leading to sudden collapse. The calculation of buckling for the web local buckling of flanged stiffeners made of flanged profiles was calculated using Eq. (11) as described in IACS-BC:

$$\sigma_{CR3} = \phi \frac{10^3 b_E\,t_{n50}\,R_{eHp} + (h_{we}\,t_{w-n50} + b_f\,t_{f-n50})R_{eHs}}{10^3 st_{n50} + h_w\,t_{w-n50} + b_f\,t_{f-n50}} \tag{11}$$

For the web local buckling of flanged stiffeners made of flanged profiles, the calculation was mainly based on effective width (b_E) and

effective height (h_{we}), where

$$b_E = \left(\frac{2.25}{\beta_E} - \frac{1.25}{\beta_E^2} \right) s \text{ for } \beta_E > 1.25 \tag{12}$$

$$b_E = s \text{ for } \beta_E \leq 1.25 \tag{13}$$

β_E was the correction factor for effective width described as:

$$\beta_E = 10^3 \frac{s}{t_{n-50}} \sqrt{\frac{\varepsilon R_{eHp}}{E}} \tag{14}$$

while

$$h_{we} = \left(\frac{2.25}{\beta_w} - \frac{1.25}{\beta_w^2} \right) h_w \text{ for } \beta_E > 1.25 \tag{15}$$

$$h_{we} = h_w \text{ for } \beta_E \leq 1.25 \tag{16}$$

β_w was the correction factor for effective height described as:

$$\beta_w = \frac{h_w}{t_{w-n50}} \sqrt{\frac{\varepsilon R_{eHs}}{E}} \tag{17}$$

β_E and β_w had almost identical formulas. This is because both formulas have the same basis, namely the β factor. β was described as [41]:

$$\beta = \frac{b}{t} \sqrt{\sigma_0/E} \tag{18}$$

- Web local buckling of stiffeners made of flat bars

The calculation of buckling for the web local buckling of stiffeners made of flat bars was calculated with Eq. (19) as described in IACS-BC:

$$\sigma_{CR4} = \phi \frac{A_{p-n50}\,\sigma_{CP} + A_{s-n50}\,\sigma_{C4}}{A_{p-n50} + A_{s-n50}} \tag{19}$$

where σ_{C4} was the critical stress and, as in beam column buckling and torsional buckling, the critical stress web local buckling of stiffeners made of flat bars was based on the Euler formula. The σ_{E4} was specified by IACS-BC as:

$$\sigma_{E4} = 160000 \left(\frac{t_{w-n50}}{h_w} \right)^2 \tag{20}$$

- Plate buckling

$$\sigma_{CR5} = \min \begin{cases} R_{eHp}\phi \\ \phi R_{eHp} \left[\frac{s}{\ell} \left(\frac{2.25}{\beta_E} - \frac{1.25}{\beta_E^2} \right) + 0.1 \left(1 - \frac{s}{\ell} \right) \left(1 + \frac{1}{\beta_E^2} \right)^2 \right] \end{cases} \tag{21}$$

As in the calculation of the web local buckling of flanged stiffeners made of flanged profiles, plate buckling is also strongly influenced by β factors. The β factors used are the same as those stated in Eq. (14). In addition, the main variable that is most influential in plate buckling is R_{eHp}. R_{eHp} is the minimum yield stress of the material of the considered plate. R_{eHp} is described by IACS-BC as:

$$R_{eHp} = \frac{R_{eHp1}\,t_{1-n50}\,s_1 + R_{eHp2}\,t_{2-n50}\,s_2}{t_{n50}\,s} \tag{22}$$

Where R_{eHp1}, R_{eHp2}, t_{1-n50}, t_{2-n50}, s_1, and s_2 are the size of the plate element affected by the stiffener effect as stated in Fig. 2.

As can be seen in Fig. 3, in the calculation of HGUS, an incremental step is propagated and an incremental curvature is applied in each incremental step. The incremental curvature is adjusted to the angle of rotation of the transverse section hull girder around the NA axis. Then, the calculation of strain and stress for each element is carried out. The
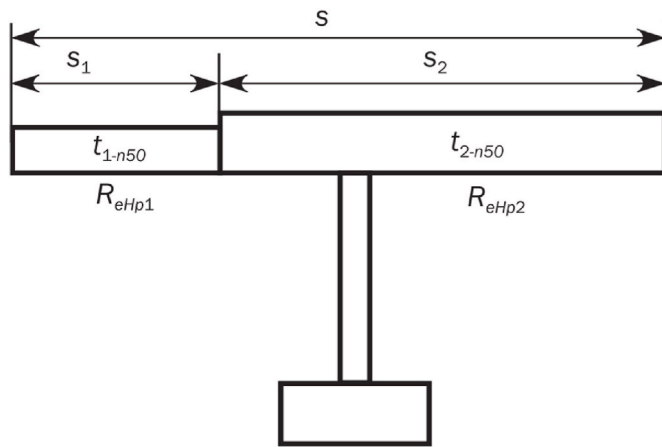
Fig. 2. Element with different thickness and yield strength.

procedure is repeated for each step with an updated NA by setting the equilibrium of the force across the transverse section. The bending moment is calculated by summing the contributions of the entire element. Furthermore, to obtain HGUS, bending moment plotting is carried out against the curvature and the HGUS value is determined as the peak value of the curve. The curve obtained is divided into two categories: under the $y = 0$ axis and above the $y = 0$ axis. Essentially, the separation of curves is divided due to the sagging and hogging conditions considered in the calculation. According to Paik and Kim [42], under sagging conditions the deck panels are mostly subjected to longitudinal axial compression, while the lower panel undergoes axial stress, longitudinal bending, and lateral pressure, and the inverse is true under hogging conditions.

5. Corrosion rate of stiffener elements of ship hull

The aging structure of a ship always consists of some damage such as corrosion, fatigue cracks, and local dents. Corrosion is the most important and serious major factor in the damage to ship structures due to aging [43]. Corrosion can appear in any zone of the ship's structure, but there are some locations that are more susceptible to corrosion, such as the inner bottom, lower and upper sloping plates, hold frames, side shell plates, deck plates, shear strakes, and longitudinal decks [44]. The growth of the corrosion of ship structural elements is spatially dependent, where the degree of corrosion reduction varies depending on the part of the ship [31]. The corrosion effect is a representation of a constant corrosion rate which results in a linear decrease in plate thickness against service time. Methods used to estimate the behavior of ship structures are usually developed for intact structures in assuming that corrosion will uniformly reduce the thickness of structural components [45].

When the percentage of the degradation of structure thickness

exceeds 20%, a decrease in the mechanical properties of the structure affected by corrosion occurs [46]. Such a decrease in mechanical properties is due to local non-uniformities in the corroded surface. In other words, if the corrosion that occurs causes the uniform depletion of the formed specimen, changes in the mechanical properties of the material exposed to corrosion can be ignored [47]. In the case of uniform corrosion, buckling or the ultimate strength of stiffened and unstiffened plates can be easily estimated by subtracting the plate thickness from its original value. There are several ways to estimate the position of the hull girder element against corrosion growth. The simplest way is to classify the parts of the vessel according to the characteristics that affect the growth of corrosion and calibrate the corrosion model separately based on the thickness measurements of the rusty plates of each different part [31,48].

As indicated in Fig. 2, the process of the corrosion of steel structures exposed to seawater is categorized into three phases, namely (a) *coating resistance*, (b) *transition to corrosion*, and (c) *increased corrosion* [37]. As demonstrated in Fig. 4, the loss of plate thickness due to the effect of corrosion growth can be expressed in the function of time (years) as stated in Eqs. (23) and (24):

$$t_{\mathrm{r}} = C_1 T_e^{C_2} \tag{23}$$

$$r_{\mathrm{r}} = C_1 C_2 T_e^{C_2 - 1} \tag{24}$$

where t_{r} = the depth of corrosion (loss of plate thickness due to corrosion) in mm; r_{r} = the corrosion rate in mm/year; T_e = the time of exposure to the structure after coating damage in years; T_e specified with $T_e = T - T_c - T_t$, where T = the vessel service time in years; T_c = the
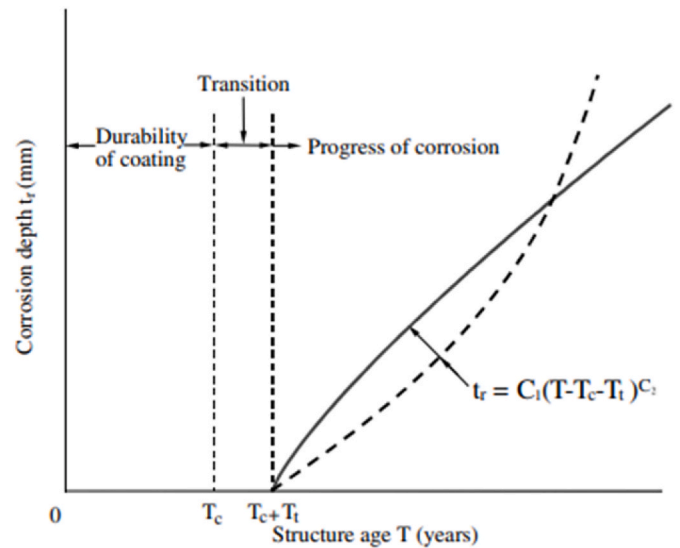

Fig. 4. A schematic of the corrosion process for marine structures.
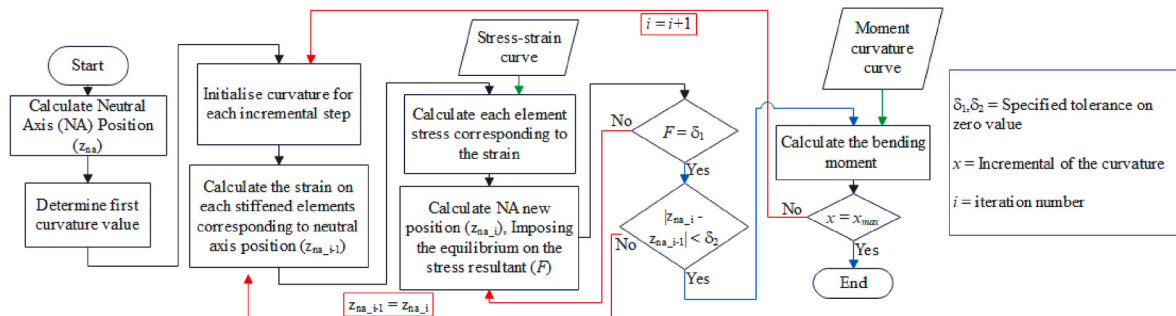

Fig. 3. Hull girder ultimate strength calculation flowchart.

coating duration in years; T_t = the duration of corrosion transition in years, with the pessimistic value taken as $T_t = 0$. C_1; and C_2 = the coefficient to be determined via the statistical analysis of the corrosion measurement data.

The durability of the coating depends on the type of coating system used, the details of its application, and the relevant maintenance. The average durability of the coating on the hull of a ship is 5–10 years [49]. After the effectiveness of the coating is lost, there is a transition time or duration between the time of losing the effectiveness of the coating and the initiation of corrosion. Transition time is often thought of as a randomized, exponentially distributed variable. Under pessimistic conditions, transition time is considered equal to zero; in other words, corrosion is assumed to occur as soon as the effectiveness of the coating is lost.

The corrosion rates used in the calculations of this study were adapted from Paik et al. [44], which were calculated based on a survey of 7503 corrosion datasets from 44 bulk carriers. The corrosion rates were then divided based on the parts of the ship as stated in Table 2, where thickness reductions on each part of the ship were considered to occur uniformly, while corrosion behavior was also divided into two conditions, namely standard corrosion rate and severe corrosion rate. The probabilistic value of the standard corrosion rate was calculated using all the data collected from corrosion inspections of ships up to 25 years old, while the severe corrosion rate was calculated using 95% and the upper limit of the total data [37].

6. Non-uniform uniaxial thrust

The thrust that works on the hull is one of the main and most fundamental variables in the determination of HGUS. Thus far, HGUS calculations based on IACS-CSR have used uniform thrust as the basis for calculation. Depending on the relative angle and vertical location of some elements based on NA, axial strain and axial displacement deviate from uniformity (non-uniform) [32]. To provide parameters and generalize the problem, non-uniform thrust is calculated using a non-dimensional displacement ratio. Using this ratio makes it easier to calculate the ultimate bending moment because the location of the NA varies based on the curvature due to progressive collapse in stiffened panels. The non-dimensional displacement ratio is formulated as Eqs. (25) and (26).

$$r_{top} = \frac{u_{top}}{u_{bot}} \qquad (25)$$

$$r_{bot} = \frac{u_{bot}}{u_{top}} \qquad (26)$$

where $0 \leq r_i \leq 1.0$ with r_i (i = top or bot).

The thrust received by the hull leads to the instability of the structure. Based on this, panel geometry generalization is required. Generalization is carried out using a slenderness ratio. Two slenderness models are used in the calculation, namely the slenderness ratio λ for stiffened panels and the slenderness ratio β for plates. The formulation of the two slenderness ratios is stated in Eqs. (27) and (28).

$$\lambda = \frac{s_t}{\pi r} \sqrt{\frac{\sigma_y}{E_m}} \qquad (27)$$

$$\beta = \frac{s}{t_p} \sqrt{\frac{\sigma_y}{E_m}} \qquad (28)$$

where:

s: longitudinal spacing
s_t: transverse stiffeners
σ_y: material's yield stress
E_m: material's Young's modulus
r: radius of gyration: $\sqrt{\frac{I}{s t_p + h_w\, t_w + b_f\, t_f}}$.

Zhang [50] conducted a study on the arrangement of stiffened panels on 46 oil tankers and bulk carrier ships and concluded that the practical ranges for both slenderness ratios were 0.05–1.0 for λ and 1.0 to 2.5 for β. Based on the above problems, an HGUS calculation is needed to consider the reciprocal relationship between the parameters associated with *stiffened panel scantlings* (λ, β) and locations corresponding to NA (r_i, θ). Thus, the value of the bending moment is expressed as follows:

$$\frac{\sigma_u}{\sigma_y} = f(r_i, \theta, \lambda, \beta) \qquad (29)$$

Based on Eq. (29), Anyfantis [32] formulated a comparative formula σ_u / σ_y that is used in estimating the influence of non-uniform uniaxial thrust on bending moment hull girders. The formula is divided into two as a representation of the displacement ratio of each element. The comparison (σ_u / σ_y) of elements with the displacement ratio r_{bot} is conducted using Eq. (30), while the element with displacement ratio r_{top} is calculated using Eq. (12) [32].

$$\frac{\sigma_u}{\sigma_y} = a_1 + a_2 \left[\frac{1}{2} + \frac{atan((r_{bot} - a_3)/a_4)}{\pi} \right] + a_5 \left[\frac{1}{2} + \frac{atan((\theta - a_6)/a_7)}{\pi} \right]$$
$$+ a_8 \left[\frac{1}{2} + \frac{atan((r_{bot} - a_3)/a_4)}{\pi} \right] \cdot \left[\frac{1}{2} + \frac{atan((\theta - a_6)/a_7)}{\pi} \right] \qquad (30)$$

$$\frac{\sigma_u}{\sigma_y} = a_1 + a_2 r_{top} + a_3\,\theta + a_4\,r_{top}^2 + a_5\,\theta^2 + a_6\,r_{top}\,\theta + a_7\,r_{top}^3 + a_8\,\theta^3$$
$$+ a_9\,r_{top}\,\theta^2 + a_{10}\,r_{top}^2\,\theta \qquad (31)$$

with a_n values specified using

$$a_n(\lambda, \beta) : C_0 + C_1\lambda + C_2\beta + C_3\lambda^2 + C_4\lambda\beta + C_5\beta^2 \qquad (32)$$

where C_n is the coefficient of the quadratic response surface obtained by adjusting λ and β. The coefficient is obtained from the regression results of Anyfantis [32] with values as shown in Table 3 for Eq. (30) and in Table 4 for Eq. (31).

Table 2
Mean value and standard distribution of corrosion rates.

No	Member Group	Standard Corrosion Rate (mm/year)		Severe Corrosion Rate (mm/year)	
		Mean	COV	Mean	COV
1	Bottom plate	0.03	0.04	0.16	0.25
2	Inner bottom plate	0.13	0.11	0.33	0.21
3	Lower sloping plate	0.08	0.08	0.29	0.21
4	Lower wing tank side shells	0.04	0.04	0.15	0.25
5	Side shells	0.05	0.07	0.15	0.23
6	Upper wing tank side shells	0.04	0.05	0.17	0.23
7	Upper sloping plate	0.04	0.03	0.16	0.23
8	Upper deck plates	0.09	0.1	0.29	0.22
9	Bottom girders	0.03	0.05	0.18	0.23
10	Outer bottom longitudinal–web	0.03	0.02	0.11	0.22
11	Outer bottom longitudinal–flange	0.03	0.02	0.15	0.24
12	Inner bottom longitudinal–web	0.03	0.04	0.14	0.2
13	Inner bottom longitudinal–flange	0.03	0.04	0.17	0.19
14	Upper wing tank side longitudinal–web	0.03	0.06	0.14	0.21
15	Upper wing tank side longitudinal–flange	0.03	0.06	0.19	0.22
16	Upper sloping longitudinal–web	0.03	0.04	0.15	0.24
17	Upper sloping longitudinal–flange	0.03	0.04	0.2	0.23
18	Upper deck longitudinal–web	0.05	0.07	0.24	0.24
19	Upper deck longitudinal–flange	0.05	0.07	0.07	0.23
20	Lower wing tank side longitudinal–web	0.02	0.03	0.07	0.18
21	Lower wing tank side longitudinal–flange	0.02	0.03	0.13	0.18
22	Lower sloping longitudinal–web	0.01	0.02	0.12	0.18
23	Lower sloping longitudinal–flange	0.01	0.02	0.14	0.21

Table 3

Coefficient C_n for r_{bot}.

	C_0	C_1	C_2	C_3	C_4	C_5
a_1	6.4464	−4.5531	−11.7874	3.3593	0.7979	3.3524
a_2	−6.5139	7.1343	13.6723	−6.3308	−0.4703	−4.0291
a_3	−0.1917	0.1749	0.2831	−0.2004	0.0043	−0.0808
a_4	0.5203	1.2859	−0.5642	−1.0542	0.0678	0.1474
a_5	−6.0357	4.3580	11.9172	−2.9266	−1.1152	−3.3330
a_6	35.6467	9.0383	−58.7719	−8.3489	3.9069	16.3199
a_7	17.2061	102.683	−41.7847	−74.7277	−9.1801	15.4037
a_8	7.3208	−6.5535	−14.0765	5.1577	0.9073	4.0337

7. Ultimate limit state (ULS)

Safety is one of the main criteria in structural design that needs to be ensured. The most important criterion for ensuring safety in structural design is the strength criterion. All structural elements must meet the necessary limits on the level of strength. The determination of strength criteria for stiffened panels is based on ultimate limit state (ULS) design technology [51]. The ULS design criterion of ship-shaped offshore unit hulls under vertical bending moments are described as presented in Equation (14) [34].

$$\frac{M_u}{\gamma_u} = \gamma_s M_{sw} + \gamma_w M_{wv} \qquad (33)$$

M_u = ultimate bending moment; M_{sw} = still-water bending moment; M_{wv} = wave-induced bending moment;

γ_u, γ_{sw}, γ_w = partial safety factors for M_u, M_{sw}, and M_{wv}, respectively.

As suggested by IACS-BC 2022, for bulk carrier hull models, the partial safety factor values used are $\gamma_{sw} = 1.0$ and $\gamma_w = 1.2$. As stated in IACS-BC, bulk carrier hull design is considered safe when γ_u is higher than 1.2. As shown by Eq. (33) in calculating the partial safety factor M_u, the values M_{sw} and M_{wv} are used. This is because as a structure that is exposed to continuous loads, the structure of a ship provides a response in terms of stress or deflection. Based on IACS-BC 2022, M_{sw} and M_{wv} are divided into two calculations according to the conditions imposed on the hull.

Minimum still water bending moment (Eqs. (34) and (35))

$$M_{sw-h-min} = f_{sw}\left(171 C_w L^2 B (C_b + 0.7) 10^{-3} - M_{wv-h-mid}\right) \text{ for hogging} \qquad (34)$$

$$M_{sw-s-min} = -0.85 f_{sw}\left(171 C_w L^2 B (C_b + 0.7) 10^{-3} + M_{wv-s-mid}\right) \text{ for sagging} \qquad (35)$$

Wave-induced bending moment (Eqs. (36) and (37))

$$M_{wv-h-mid} = 0.19 f_{nl-vh} f_m f_p C_w L^2 B C_b \text{ for hogging} \qquad (36)$$

$$M_{wv-s-mid} = -0.19 f_{nl-vs} f_m f_p C_w L^2 B C_b \text{ for sagging} \qquad (37)$$

Both deformations are based on Murray's method. Murray's method is based on the idea that forces and moments in a ship are self-balancing or that no net force or moment is transferred to the world. The wave-induced bending moment is given as a function of ship breadth (B)

and length (L) as shown in Eq. (38):

$$M_w = b_c \cdot B \cdot L^{2.5} \times 10^{-3} \text{ tonnes metres} \qquad (38)$$

where b_c has a value equivalent to a coefficient block (C_b). If the still water bending moment is not available, it can be obtained using Eq. (39).

$$M_s = \frac{W_F W_A}{2} - \frac{W}{2} L \cdot C_b \cdot B \qquad (39)$$

8. Results and discussion

The HGUS value was obtained using numerical analysis methods with the help of an in-house program that was based on IACS-CSR's incremental–iterative method. The HGUS value was obtained by considering the effect of standard and severe corrosion at 0, 10, 15, and 20 years and by considering the non-uniform uniaxial thrust before checking the safety level using ULS parameters.

8.1. Non-uniform thrust

In the bulk carrier hull girder model used, there were 46 stiffeners experiencing r_{bot} conditions and 44 stiffeners experiencing r_{top} conditions. In each stiffener, the value $r_i = 1$ was used as a representation of almost evenly distributed values of r_i in each stiffener. The value θ was determined according to the condition of the slope of the stiffener against NA with minimum and maximum values as $0° \leq \theta \leq 90°$. As stated in Table 5, the value σ_u / σ_y in section r_{bot} was greater than that of section r_{top}. The low value σ_u / σ_y in section r_{top} was in line with the high standard deviation in section r_{top}.

With the bulk carrier hull model considering non-uniform uniaxial thrust, the value of HGUS decreased compared with that of HGUS with uniform thrust. As shown in Fig. 5, HGUS decline occurred both in hogging and sagging conditions. The shape of the graph tends to be the same both in the hogging and sagging conditions. This is because the spread of stiffeners affected by the non-uniform uniaxial thrust effect was evenly distributed. However, there was a significant decrease in the bending moment at a curvature of 0.14×10^{-3} m^{-1} in the hogging condition and at 0.11×10^{-3} m^{-1} in the sagging condition. These results were consistent with the results of Anyfantis [32], which stated that non-uniform uniaxial thrust decreased the yield strength of stiffened panels, leading to a decrease in the hull girder ultimate strength of the ship hull.

8.2. Corrosion effect

Reduction in thickness in ship structures is associated with the results of the research by Paik et al. [44] listed in Table 1 where the corrosion effect is divided into two types and the decrease in thickness of each element at the same location under the same conditions occurs uniformly. In this study, 0, 10, 15, and 20 years of service times were used based on the average lifespan of ships according to UNCTAD [52], which

Table 4

Coefficient C_n for r_{top}.

	C_0	C_1	C_2	C_3	C_4	C_5
a_1	1.1478	0.6693	−0.4522	−0.7049	0.0722	0.0633
a_2	0.6147	−1.07062	−0.1045	0.7288	−0.0404	0.0688
a_3	−0.0006	−0.02904	5.343 E−03	0.013978	1.564 E−03	−0.0013
a_4	−0.6166	0.6891	0.28001	−0.8511	0.1019	−0.1126
a_5	−3.64 E−05	2.07 E−04	−5.52 E−05	1.22 E−05	−6.10 E−05	2.95 E−05
a_6	−0.00216	0.02902	2.388 E−03	−0.01771	1.012 E−03	−1.73 E−03
a_7	0.0964	−0.4302	0.01623	0.577213	−0.0555	9.999 E−03
a_8	2.36 E−07	−1.73E−07	2.11 E−07	−5.89 E−07	2.93 E−07	−1.57 E−07
a_9	1.22 E−05	−1.9 E−04	1.53 E−05	6.20 E−05	2.29 E−05	−5.51 E−06
a_{10}	3.417 E−03	−3.8 E−04	−0.00619	1.412 E−03	−0.00129	2.169 E−07

Table 5

σ_u/σ_y range value at stiffeners affected by non-uniform uniaxial thrust.

Hull Model	Conditions	Num. of Stiffeners	Bending Moment (σ_u/σ_y) Value			
			Maximum	Minimum	Mean	Std. Deviation
Bulk carrier	r_{bot}	46	0.8655	0.7490	0.8154	0.0275
	r_{top}	44	0.7509	0.2997	0.5227	0.1793

(a)   (b)
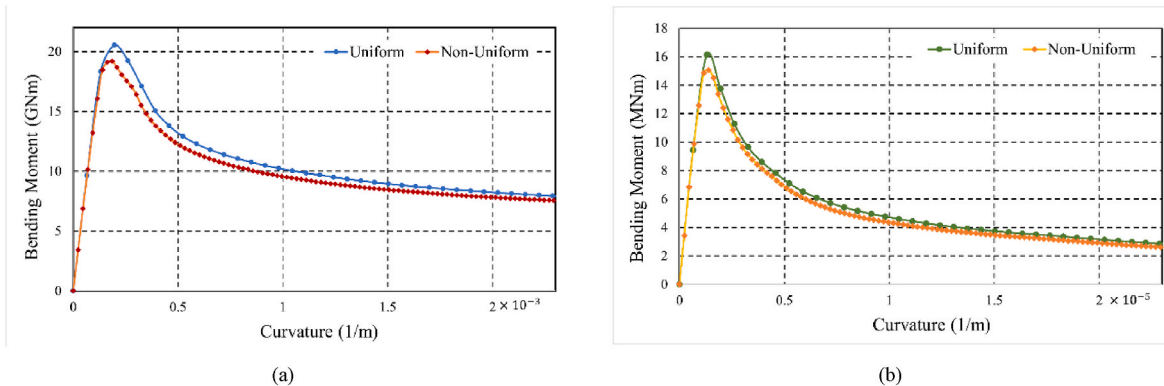
Fig. 5. Hull girder ultimate strength with: (a) hogging and (b) sagging.

is 21.29 years. In addition, in this study, the durability of the coating for 5 years and a transition time of zero were used. As stated in Table 6, the decrease in thickness in each condition increased with each increase in service time. At a service time of 20 years, this decrease was smaller in the standard condition than in severe conditions even where the severe condition service time was 10 years.

After experiencing a decrease in thickness as a result of the corrosion rate, the stiffener on the hull girder was taken into account for its inclination effect. The calculation of the inclination effect is carried out by the formulation of a non-uniform uniaxial thrust as formulated in Eq. (29). As stated in Table 7, σ_u/σ_y conditions without being exposed to corrosion had an average value of 0.8154 in the r_{bot} condition and 0.5227 in the r_{top} condition. Those σ_u/σ_y values continued to experience an increase with each service time in each corrosion rate condition. Inversely proportional to the decrease of thickness, the σ_u/σ_y value in severe conditions with a service time of 10 years was greater than that in standard conditions with a service time of 20 years.

Following the decrease in thickness in each element as a result of the corrosion rate, the HGUS value at each service time in each condition also decreased. As shown in Fig. 6, the HGUS value decreased with a linear trend following service time both in the hogging and sagging conditions. Moreover, in both the hogging and sagging conditions, the decrease rate with severe corrosion appeared more extreme than the rate with standard corrosion. The decrease in HGUS due to the effect of non-uniform uniaxial thrust at each service time resembled a decrease in HGUS with a uniform thrust effect in both the hogging and sagging conditions. This occurred because, as stated in Table 7, the average value of σ_u/σ_y tended to be the same among each corrosion rate condition at each service time.

As shown in Table 8, the percentage decrease in HGUS in the hogging condition was greater than that in the sagging condition. This occurred evenly in each corrosion rate condition at each service time. These results are consistent with the report by Gao et al. [35] which stated that

uniform corrosion has the greatest effect in reducing ultimate strength on hogging conditions as opposed to sagging conditions.

As stated in Figs. 7 and 8, the decrease in the bending moment does not only occur in the ultimate part; the decrease in the bending moment due to the corrosion effect occurs evenly in each increment as is demonstrated by the similar trends in the graphic. A decline occurred across the board both in hogging and sagging conditions as well as with uniform and non-uniform uniaxial thrust. The shape of the graphic seems to have arisen from reductions in plate thickness since the corrosion effect occurred in all hull elements.

8.3. Ultimate limit state (ULS)

ULS is the main parameter in determining the safety level of a ship's structural design. The design of a ship's structure is considered safe if the γ_u value is greater than equal to 1.2 ($\gamma u > 1.2$). As stated in Table 9, as the HGUS decreased, the average γ_u value in each corrosion condition at each service time also decreased. In addition to occurring in each corrosion rate condition, the decrease also occurred due to the influence of non-uniform uniaxial thrust. The γ_u value difference in the hull girder affected by non-uniform uniaxial thrust was 6.68% for hogging and 6.62% for sagging conditions. A γ_u value of less than 1.2 was found only in sagging conditions with a severe corrosion rate. Only a severe corrosion rate with 10 years of service time exposed to uniform axial thrust exhibited a γ_u value higher than 1.2. This indicates that the structure of a ship that is exposed to severe corrosion conditions is in a very vulnerable condition due to the rapid decrease in thickness. It is highly recommended that the current methodology be applied in order to investigate other critical topics, e.g., the HGUS calculation of hull structures under various damaged conditions [53–55] that partly or largely destroy structural members. Furthermore, the ultimate strength of stiffened panels based on non-steel materials is a potential future topic of interest since composites, polymers, and other viable advanced

Table 6

Thickness reduction affected by corrosion value at each corrosion condition.

	Standard 10	Standard 15	Standard 20	Severe 10	Severe 15	Severe 20
Mean	**0.218**	**0.436**	**0.654**	**0.924**	**1.848**	**2.772**
Std. deviation	0.153	0.307	0.460	0.312	0.624	0.935

Table 7

σ_u/σ_y range value of stiffeners affected by non-uniform uniaxial thrust in each corrosion condition.

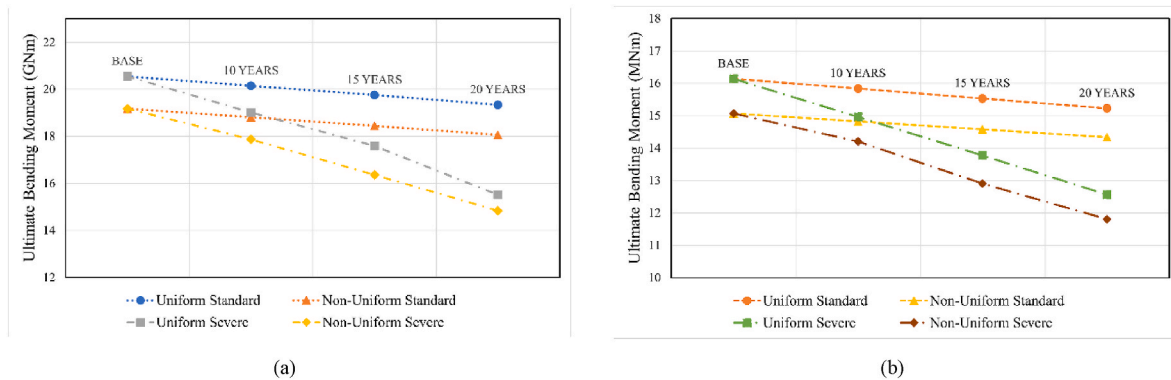| Corrosion Condition	Conditions	Bending Moment (σ_u/σ_y) Value				% σ_u/σ_y Reduction
		Maximum	Minimum	Mean	Std. Deviation	
Base	r_{bot}	0.8655	0.7490	0.8154	0.0275	N/A
	r_{top}	0.7509	0.2997	0.5227	0.1793	N/A
Standard 10	r_{bot}	0.8641	0.7464	0.8121	0.0278	**0.40%**
	r_{top}	0.7445	0.2941	0.5170	0.1790	**1.09%**
Standard 15	r_{top}	0.8628	0.7438	0.8087	0.0281	**0.83%**
	r_{bot}	0.7379	0.2884	0.5112	0.1786	**2.21%**
Standard 20	r_{top}	0.8614	0.7411	0.8051	0.0285	**1.27%**
	r_{top}	0.7310	0.2827	0.5053	0.1782	**3.34%**
Severe 10	r_{bot}	0.8595	0.7357	0.8004	0.0292	**1.84%**
	r_{top}	0.7261	0.2655	0.4952	0.1832	**5.27%**
Severe 15	r_{bot}	0.8530	0.7209	0.7827	0.0317	**4.01%**
	r_{top}	0.6987	0.2308	0.4661	0.1862	**10.84%**
Severe 20	r_{bot}	0.8461	0.7046	0.7628	0.0338	**6.45%**
	r_{top}	0.6684	0.1969	0.4359	0.1879	**16.62%**

Fig. 6. Hull girder ultimate strength value reduction in each corrosion condition with: (a) hogging and (b) sagging.

Table 8

HGUS percentage reduction in each corrosion condition.

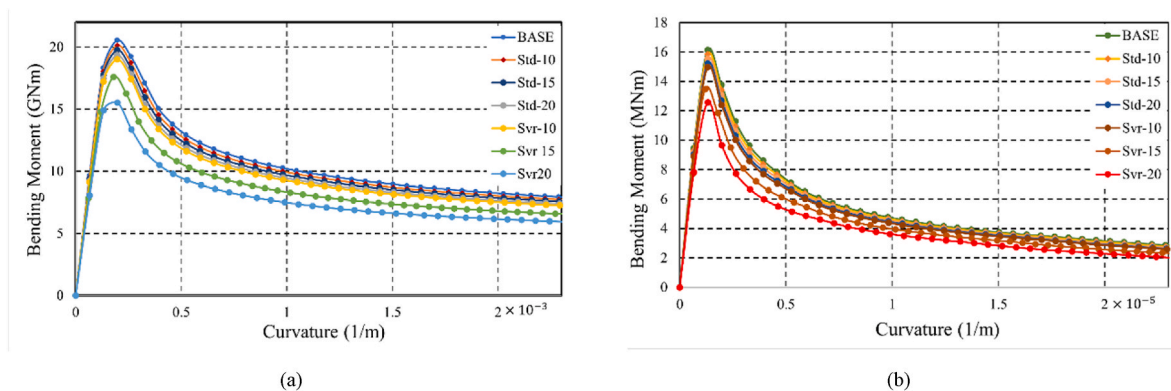|		Standard 10	Standard 15	Standard 20	Severe 10	Severe 15	Severe 20
Uniform	Hogging	1.96%	3.86%	5.87%	7.47%	14.39%	24.48%
	Sagging	1.85%	3.74%	5.64%	7.27%	14.65%	22.12%
Non-Uniform	Hogging	1.89%	3.82%	5.81%	6.83%	14.65%	22.64%
	Sagging	1.63%	3.25%	4.87%	5.74%	14.37%	21.62%

Fig. 7. Hull girder ultimate strength of uniform thrust with: (a) hogging and (b) sagging.

materials are projected to become alternative structural and engineering materials [56–59].

9. Conclusions

In this study, HGUS calculations were carried out for a bulk carrier hull model. HGUS calculations were carried out in hogging and sagging
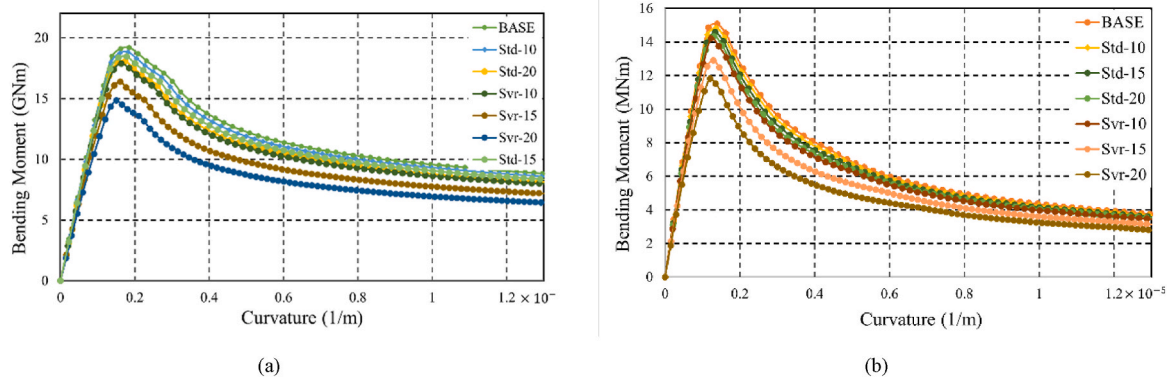
Fig. 8. Hull girder ultimate strength of non-uniform uniaxial thrust with: (a) hogging and (b) sagging.

Table 9
Ultimate limit state for each corrosion condition HGUS.<–Q4: For this **Table 9**, please provide a definition for the significance of [bold]. Either provide a legend through the "Comment" option at the top of your article page or add a footnote.>

γu Uniform							
	Base	Standard 10	Standard 15	Standard 20	Severe 10	Severe 15	Severe 20
Hogging	1.652	1.619	1.588	1.555	1.528	1.414	1.247
Sagging	1.351	1.326	1.301	1.275	1.253	**1.153**	**1.052**
γu Non-uniform							
	Base	Standard 10	Standard 15	Standard 20	Severe 10	Severe 15	Severe 20
Hogging	1.541	1.512	1.482	1.452	1.436	1.315	1.192
Sagging	1.262	1.241	1.221	1.200	**1.189**	**1.080**	**0.989**

conditions using Smith's method referring to IACS-CSR 2022. The location standard and corrosion rate severity conditions changed depending on those given to each element at 0, 10, 15, and 20 service times. Moreover, depending on the relative angle and vertical location of each element with respect to NA, the axial strain and axial displacement deviated from uniformity (non-uniform). As such, the calculation of HGUS was divided into two further conditions: with and without the consideration of non-uniform uniaxial thrust.

Based on the results of the HGUS calculation in each thrust condition, there was a decrease in the maximum value of the bending moment in the hogging and sagging conditions when non-uniform uniaxial thrust was considered. This shows that non-uniform uniaxial thrust has a negative influence on HGUS. Based on the HGUS results considering the corrosion rate, severe corrosion rates more negatively affected HGUS even with a lower service time. The corrosion rate effect was higher in the hogging condition than in the sagging condition. Based on the ULS calculation, all the standard corrosion rate conditions had a value higher than 1.2 γ_u, while nearly all the severe corrosion rate conditions with sagging conditions had a value less than 1.2 γ_u. With respect to recommendations for further research, future studies need to consider the non-uniform uniaxial thrust effect on all stiffened elements and not only on tee stiffener elements. In addition, values of r_i should be updated for each iteration so that the calculation of the influence of non-uniform uniaxial thrust may be more accurate.

Credit author statement

Imaduddin Faqih: Conceptualization; Investigation; Formal analysis; Validation; Methodology; Data curation; Writing – original draft. **Ristiyanto Adiputra**: Supervision; Conceptualization; Investigation; Supervision; Writing – original draft; Project administration. **Aditya Rio Prabowo**: Supervision; Writing – original draft; Writing – review & editing; Software; Funding acquisition; Project administration. **Nurul Muhayat**: Supervision; Conceptualization; Methodology; Writing – original draft; Funding acquisition. **Sören Ehlers**: Supervision; Conceptualization; Methodology; Visualization; Writing – review & editing. **Moritz Braun**: Supervision; Conceptualization; Methodology; Visualization; Writing – review & editing.

Declaration of competing interest

The authors declare that they have no known competing financial interests or personal relationships that could have appeared to influence the work reported in this paper.

Data availability

The authors do not have permission to share data.

Acknowledgements

References

[1] H. Nubli, A. Fajri, A.R. Prabowo, Khaeroman, J.M. Sohn, CFD implementation to mitigate the LNG leakage consequences: a review of explosion accident calculation on LNG-fueled ships, Procedia Struct. Integr. 41 (2022) 343–350, https://doi.org/10.1016/j.prostr.2022.05.040.

[2] H. Nubli, J.M. Sohn, A.R. Prabowo, Layout optimization for safety evaluation on LNG-fueled ship under an accidental fuel release using mixed-integer nonlinear programming, Int. J. Nav. Archit. Ocean Eng. 14 (2022), 100443, https://doi.org/10.1016/j.ijnaoe.2022.100443.

[3] A. Fajri, A.R. Prabowo, N. Muhayat, Assessment of ship structure under fatigue loading: FE benchmarking and extended performance analysis, Curve, Layer. Struct. 9 (2022) 163–186, https://doi.org/10.1515/cls-2022-0014.

[4] M. Yusvika, A. Fajri, T. Tuswan, A.R. Prabowo, S. Hadi, I. Yaningsih, T. Muttaqie, F.B. Laksono, Numerical prediction of cavitation phenomena on marine vessel:

effect of the water environment profile on the propulsion performance, Open Eng. 12 (2022) 293–312, https://doi.org/10.1515/eng-2022-0034.

[5] M. Yusvika, A.R. Prabowo, D.D.D.P. Tjahjana, J.M. Sohn, Cavitation prediction of ship propeller based on temperature and fluid properties of water, J. Mar. Sci. Eng. 8 (2020) 465, https://doi.org/10.3390/jmse8060465.

[6] A.R. Prabowo, B. Cao, J.M. Sohn, D.M. Bae, Crashworthiness assessment of thin-walled double bottom tanker: influences of seabed to structural damage and damage-energy formulae for grounding damage calculations, J. Ocean Eng. Sci. 5 (2020) 387–400, https://doi.org/10.1016/j.joes.2020.03.002.

[7] A.R. Prabowo, D.M. Bae, Environmental risk of maritime territory subjected to accidental phenomena: correlation of oil spill and ship grounding in the Exxon Valdez's case, Res. Eng. 4 (2019), 100035, https://doi.org/10.1016/j.rineng.2019.100035.

[8] R. Adiputra, T. Utsunomiya, Stability based approach to design cold-water pipe (CWP) for ocean thermal energy conversion (OTEC), Appl. Ocean Res. 92 (2019), 101921, https://doi.org/10.1016/j.apor.2019.101921.

[9] M.Z.M. Alie, D. Ramasari, T. Rachman, R. Adiputra, Effects of collision damage on the ultimate strength of FPSO vessels, Makara J. Technol. 24 (2020) 1–6, https://doi.org/10.7454/mst.v24i1.3732.

[10] R.I. Julianto, T. Muttaqie, R. Adiputra, S. Hadi, R.L.L.G. Hidajat, A.R. Prabowo, Hydrodynamic and structural investigations of catamaran design, Procedia Struct. Integr. 27 (2020) 93–100, https://doi.org/10.1016/j.prostr.2020.07.013.

[11] A.R. Prabowo, T. Tuswan, R. Adiputra, Q.T. Do, J.M. Sohn, E. Surojo, F. Imaduddin, Mechanical behavior of thin-walled steel under hard contact with rigid seabed rock: theoretical contact approach and nonlinear FE calculation, J. Mech. Behav. Mater. 30 (2021) 156–170, https://doi.org/10.1515/jmbm-2021-0016.

[12] A.R. Prabowo, T. Tuswan, R. Ridwan, Advanced development of sensors' roles in maritime-based industry and research: from field monitoring to high-risk phenomenon measurement, Appl. Sci. 11 (2021) 3954, https://doi.org/10.3390/app11093954.

[13] D.T.A. Ansori, A.R. Prabowo, T. Muttaqie, N. Muhayat, F.B. Laksono, D.D.D. P. Tjahjana Prasetyo, Y. Kuswardi, Investigation of honeycomb sandwich panel structure using aluminum alloy (AL6XN) material under blast loading, Civ. Eng. J. 8 (2022) 1046–1068, https://doi.org/10.28991/CEJ-2022-08-05-014.

[14] Lloyd's List Intelligence, Casualty Statistics, Informa UK Limited, London, 2021.

[15] EMSA, Annual Overview of Marine Casualties and Incidents 2021, European Marine Safety Agency, Lisbon, 2021.

[16] J.K. Paik, D.K. Kim, D.H. Park, H.B. Kim, A.E. Mansour, J.B. Caldwell, Modified Paik–Mansour formula for ultimate strength calculations of ship hulls, Ships Offshore Struct. 8 (2012) 245–260, https://doi.org/10.1080/17445302.2012.676247.

[17] R. Adiputra, T. Yoshikawa, E. Erwandi, Reliability-based assessment of ship hull girder ultimate strength, curve, Layer. Struct. 10 (2023), 20220189, https://doi.org/10.1515/cls-2022-0189.

[18] D.K. Kim, H.L. Lim, S.Y. Yu, A technical review on ultimate strength prediction of stiffened panels in axial compression, Ocean. Eng. 170 (2018) 392–406, https://doi.org/10.1016/j.oceaneng.2018.10.022.

[19] J.B. Caldwell, Ultimate longitudinal strength, Trans. RINA 107 (1965) 411–430.

[20] C.S. Smith, Influence of local compressive failure on ultimate longitudinal strength of a ship's hull, in: Proceedings of International Symposium on Practical Design in Shipbuilding, 1977, pp. 73–79.

[21] Y. Ueda, S.M.H. Rashed, An ultimate transverse strength analysis of ship structures, J. Soc. Nav. Archit. Jpn. 136 (1974) 309–324, https://doi.org/10.2534/jjasnaoe1968.1974.136_309.

[22] M. Zunita, Y.J. Kevin, Ionic liquids as corrosion inhibitor: from research and development to commercialization, Res. Eng. 15 (2022), 100562, https://doi.org/10.1016/j.rineng.2022.100562.

[23] J.K. Paik, A.K. Thayamballi, Ultimate Limit State Design of Steel-Plated Structures, John Wiley & Sons, Inc, New Jersey, 2003.

[24] D. Douche, H. Elmsellem, E.H. Anouar, L. Guo, B. Hafez, B. Tüzün, A. El Louzi, K. Bougrin, K. Karrouchi, B. Himmi, Anti-corrosion performance of 8-hydroxy-quinoline derivatives for mild steel in acidic medium: gravimetric, electrochemical, DFT and molecular dynamics simulation investigations, J. Mol. Liq. 308 (2020), 113042, https://doi.org/10.1016/j.molliq.2020.113042.

[25] K. Chkirate, K. Azgaou, H. Elmsellem, B. El Ibrahimi, N. Sebbar, E.H. Anouar, M. Benmessaoud, S. El Hajjaji, E.M. Essassi, Corrosion inhibition potential of 2-[(5-methylpyrazol-3-yl) methyl] benzimidazole against carbon steel corrosion in 1 M HCl solution: combining experimental and theoretical studies, J. Mol. Liq. 321 (2021), 114750, https://doi.org/10.1016/j.molliq.2020.114750.

[26] H. Elmsellem, H. Nacer, F. Halaimia, A. Aouniti, I. Lakehal, A. Chetouani, S.S. Al-Deyab, I. Warad, R. Touzani, B. Hammouti, Anti-corrosive properties and quantum chemical study of (E)-4-Methoxy-N-(Methoxybenzylidene) aniline and (E)-N-(4-Methoxybenzylidene)-4-Nitroaniline coating on mild steel in molar hydrochloric, Int. J. Electrochem. Sci. 9 (2014) 5328–5351, https://doi.org/10.13140/RG.2.1.4505.2326.

[27] B. Hafez, M. Mokhtari, H. Steli, Environmentally friendly inhibitor of the corrosion of mild steel: commercial oil of Eucalyptus, Int. J. Corros. Scale Inhib. 8 (2019) 573–585, https://doi.org/10.17675/2305-6894-2019-8-3-3.

[28] H. Elmsellem, Y.E. Ouadi, M. Mokhtari, H. Bendaif, H. Steli, A. Aouniti, A. M. Almehdi, I. Abdel-Rahman, H.S. Kusuma, B. Hammouti, A natural antioxidant and an environmentally friendly inhibitor of mild steel corrosion: a commercial oil of basil (ocimum basilicum L.), J. Chem. Technol. Metall. 54 (2019) 742–749.

[29] L. Toukal, D. Belfennache, M. Foudia, R. Yekhlef, F. Benghanem, B. Hafez, H. Elmsellem, I. Abdel-Rahman, Inhibitory power of N,Ń-(1,4-phenylene)bis(1-(4-nitrophenyl) methanimine) and the effect of the addition of potassium iodide on

the corrosion inhibition of XC70 steel in HCl medium: theoretical and experimental studies, Int. J. Corros. Scale Inhib. 11 (2022) 438–464, https://doi.org/10.17675/2305-6894-2022-11-1-26.

[30] S. Attabi, M. Mokhtari, Y. Taibi, I. Abdel-Rahman, B. Hafez, H. Elmsellem, Electrochemical and tribological behavior of surface-treated titanium alloy Ti–6Al–4V, J. Bio. Tribo. Corros. 5 (2019) 2, https://doi.org/10.1007/s40735-018-0193-5.

[31] A. Zayed, Y. Garbatov, C.G. Soares, Corrosion degradation of ship hull steel plates accounting for local environmental conditions, Ocean. Eng. 163 (2018) 299–306, https://doi.org/10.1016/j.oceaneng.2018.05.047.

[32] K.N. Anyfantis, Ultimate strength of stiffened panels subjected to non-uniform thrust, Int. J. Nav. Archit. Ocean Eng. 12 (2020) 325–342, https://doi.org/10.1016/j.ijnaoe.2020.03.003.

[33] K.N. Anyfantis, Ultimate compressive strength of eccentrically loaded stiffened panels in ship structures: A computational study, in: Proceedings of the 38th International Conference on Ocean, Offshore & Arctic Engineering, Glasgow, 2019, https://doi.org/10.1115/OMAE2019-96708.

[34] J.K. Paik, A.K. Thayamballi, Ship-Shaped Offshore Installations, Cambridge University Press, New York, 2007.

[35] D.W. Gao, G.J. Shi, D.Y. Wang, Residual ultimate strength of hull structures with crack and corrosion damage, Eng. Fail. Anal. 25 (2012) 316–328, https://doi.org/10.1016/j.engfailanal.2012.05.003.

[36] G.J. Shi, D.Y. Wang, B. Hu, S.J. Cai, Effect of initial geometric imperfections on dynamic ultimate strength of stiffened plate under axial compression for ship structures, Ocean. Eng. 256 (2022), 111448, https://doi.org/10.1016/j.oceaneng.2022.111448.

[37] J.K. Paik, A.K. Thayamballi, Y.I. Park, J.S. Hwang, A time-dependent corrosion wastage model for bulk carrier structures, Trans. Royal Inst. Naval Archit. Part A: Int. J. Marit. Eng. 145 (2003) 61–87, https://doi.org/10.3940/rina.ijme.2003.a2.18031.

[38] H. Ohtsubo, Y. Sumi, Proceedings of the 14th International Ship and Offshore Structures Congress, Elsevier Science, Oxford, 2000.

[39] IACS-BC, Common Structural Rules for Bulk Carriers and Oil Tankers, International Association of Classification Societies, London, 2022.

[40] Det Norske Veritas, Buckling Strength Analysis, Classification Notes No. 30.1, Det Norske Veritas, Høvik, 1995.

[41] E.V. Lewis, Principles of Naval Architecture: Second Revision, The Society of Naval Architects and Marine Engineers, New Jersey, 1988.

[42] J.K. Paik, B.J. Kim, Ultimate strength formulations for stiffened panels under combined axial load, in-plane bending and lateral pressure: a benchmark study, Thin-Walled Struct. 40 (2002) 45–83, https://doi.org/10.1016/S0263-8231(01)00043-X.

[43] D.K. Kim, D.K. Park, H.B. Kim, J.K. Seo, B.J. Kim, J.K. Paik, M.S. Kim, The necessity of applying the common corrosion addition rule to container ships in terms of ultimate longitudinal strength, Ocean. Eng. 49 (2012) 43–55, https://doi.org/10.1016/j.oceaneng.2012.04.012.

[44] J.K. Paik, S.K. Kim, S.K. Lee, Probabilistic corrosion rate estimation model for longitudinal strength members of bulk carriers, Ocean. Eng. 25 (1998) 837–860, https://doi.org/10.1016/S0029-8018(97)10009-9.

[45] K. Woloszyk, Y. Garbatov, Advances in modelling and analysis of strength of corroded ship structures, J. Mar. Sci. Eng. 10 (2022) 807, https://doi.org/10.3390/jmse10060807.

[46] Y. Garbatov, C.G. Soares, J. Parunov, J. Kodvanj, Tensile strength assessment of corroded small scales specimens, Corrosion Sci. 85 (2014) 296–303, https://doi.org/10.1016/j.corsci.2014.04.031.

[47] Y.G. Du, L.A. Clark, A.H.C. Chan, Residual capacity of corroded reinforcing bars, Mag. Concr. Res. 57 (2005) 135–147, https://doi.org/10.1680/macr.2005.57.3.135.

[48] G. Wang, J. Spencer, H. Sun, Assessment of corrosion risks to aging ships using an experience database, J. Offshore Mech. Arctic Eng. 127 (2003) 167–174, https://doi.org/10.1115/1.1894404.

[49] R. Løseth, G. Sekkesæter, S. Valsgård, Economics of high tensile steel in ship hulls, Mar. Struct. 7 (1994) 31–50, https://doi.org/10.1016/0951-8339(94)90009-4.

[50] S. Zhang, A review and study on ultimate strength of steel plates and stiffened panels in axial compression, Ships Offshore Struct. 11 (2016) 81–91, https://doi.org/10.1080/17445302.2014.992610.

[51] J.K. Paik, A.K. Thayamballi, Some recent developments on ultimate limit state design technology for ships and offshore structures, Ships Offshore Struct. 1 (2006) 99–116, https://doi.org/10.1533/saos.2006.0110.

[52] UNCTAD, Review of Maritime Transport 2020. Technical Report, United Nations Conference on Trade and Development, United Nations Publications, New York, 2020.

[53] A.A. Pratama, A.R. Prabowo, T. Muttaqie, N. Muhayat, R. Ridwan, B. Cao, F. B. Laksono, Hollow tube structures subjected to compressive loading: implementation of the pitting corrosion effect in nonlinear FE analysis, J. Braz. Soc. Mech. Sci. Eng. 45 (2023) 143, https://doi.org/10.1007/s40430-023-04067-3.

[54] Q.T. Do, T. Muttaqie, P.T. Nhut, M.T. Vu, N.D. Khoa, A.R. Prabowo, Residual ultimate strength assessment of submarine pressure hull under dynamic ship collision, Ocean. Eng. 266 (2022), 112951, https://doi.org/10.1016/j.oceaneng.2022.112951.

[55] A. Suyuthi, B.J. Leira, K. Riska, Fatigue damage of ship hulls due to local ice-induced stresses, Appl. Ocean Res. 42 (2013) 87–104, https://doi.org/10.1016/j.apor.2013.05.003.

[56] H.I. Akbar, E. Surojo, D. Ariawan, A.R. Prabowo, Experimental study of quenching agents on Al6061–Al2O3 composite: effects of quenching treatment to

microstructure and hardness characteristics, Res. Eng. 6 (2020), 100105, https://doi.org/10.1016/j.rineng.2020.100105.

[57] S. Sakuri, E. Surojo, D. Ariawan, A.R. Prabowo, Experimental investigation on mechanical characteristics of composite reinforced cantala fiber (CF) subjected to microcrystalline cellulose and fumigation treatments, Compos. Commun. 21 (2020), 100419, https://doi.org/10.1016/j.coco.2020.100419.

[58] D. Ariawan, T.S. Rivai, E. Surojo, S. Hidayatulloh, H.I. Akbar, A.R. Prabowo, Effect of alkali treatment of Salacca Zalacca fiber (SZF) on mechanical properties of HDPE composite reinforced with SZF, Alex. Eng. J. 59 (2020) 3981–3989, https://doi.org/10.1016/j.aej.2020.07.005.

[59] D.F. Smaradhana, A.R. Prabowo, A.N.F. Ganda, Exploring the potential of graphene materials in marine and shipping industries –A technical review for prospective application on ship operation and material-structure aspects, J. Ocean Eng. Sci. 6 (2021) 299–316, https://doi.org/10.1016/j.joes.2021.02.004.